NON-NEWTONIAN NATURAL-CONVECTION COOLING OF A HEAT SOURCE OF VARIABLE LENGTH AND POSITION PLACED AT THE BOTTOM OF A SQUARE CAVITY

by

Abderrahmane HORIMEK*

Mechanical Engineering Department, FST, Ziane Achour University, Djelfa, Algeria

Original scientific paper
https://doi.org/10.2298/TSCI TSCI220531059H

Natural-convection cooling of a heat source placed at the bottom wall of a square cavity filled with non-Newtonian fluid was investigated numerically. Two thermal conditions were assumed at the source (imposed temperature or flux density). The effects of Rayleigh number, rheological index, n, source length, SL, its position, D, and Prandtl number, were analyzed. For a centered source. The three first parameters were varied. The results show an increase in dynamic and thermal fields' perturbations when Rayleigh number increases and/or source length increases and/or n decreases. These observations are clearer in the first heating type compared to the second. Mean Nusselt number increase is recorded when Rayleigh number increases and/or n decreases, while it decreases with source length increase until SL = 1.0 where a new increase is recorded. For a non-centered source, the previous observations still valid, noting the loss of symmetry. The highest mean rate of heat exchange is recorded when D = 0.0 with decreasing amounts when moving towards the center. Finally, Prandtl number effect is analyzed. Results show a better diffusion of heat when increases for low n. Consequently, a marked increase in the mean Nusselt number for n < 1.0, weak for n = 1.0 and almost absent for n > 1.0 are recorded with a clearer effect for the first type of heating.

Key words: *natural-convection, square cavity, Rayleigh number, source length, source position, n-index, Prandtl number*

Introduction

Cooling processes of hot parts is essential in many areas in practice, whether it is to increase efficiency by reducing losses through their exploitation, or to protect the parts against deterioration if the heat increases more and more or remains constant for a long time. The present work goes in the last axis, where a heat source is supposed to be cooled by the placement of a square cavity filled with a fluid on it, by exploiting the thermo-physical properties (density) to generate a convection flow inside the cavity without the need for an external organ (pump, fan*, etc.*). In an earlier work [1], we assumed the case of a Newtonian fluid whose objective was to exploit the geometric aspect by changing the source length and position in simulations. For greater clarity, in practice the characteristics of the source are known (size, heating type*, etc.*), and the cavity will be adapted according to them. So, after having treated and analyzed the geometrical aspect, in this work, we change the type of the confined fluid to assure him, in addition, a rheological behavior (variation of the viscosity with the shearing), which will modify the friction between the fluid layers and near-walls. This change will directly affect the

* Author's e-mails: Horimekaer4g@gmail.com, a.horimek@univ-djelfa.dz

shape and the intensity of the convective flow and therefore, the cooling process. A fluid with non-constant viscosity is known as a non-Newtonian. A very large family, hence the large number of mathematical models describing the variation of viscosity. In our work, we considered the case of a fluid obeying the so-called Ostwald-de-Waele law and often known as the power law model. Among the fluids following this law we cite: blood, molten polymers, detergents, cooling fluid, cements, printing inks, concentrated suspensions of starch*, etc.*

Natural-convection inside a cavity is widely treated in literature with different considerations. Consequently, we will present a synthesis of works very close to ours only. For a Newtonian fluid which is considered as a benchmark case- we cite the work of Rahal *et al*. [2], dealing with electronic component cooling using an air-filled cavity. The thermal flux released by Joule effect at the source is assumed to be periodic (3.5 W/m² or 0.0 W/m² each time step). Numerous results showing the effect of Rayleigh number and the time step (half period) and the source (s) situations have been provided. Still for the same objective, Banerjee *et al*. [3] analyzed the effect of heat flux intensity released by the source on both dynamic and thermal fields, in addition the average rate of heat transfer ($\overline{\mathrm{Nu}}$). Seddiki *et al*. [4] assumed the case of a hotplate under constant hot temperature, T_{H}, for the same conditions on walls assumed in [2]. The provided results show the effect of centered source length, SL, ranging from 0.2-0.8 for Ra = 10^{+5} and that of Rayleigh number for SL = 0.4. A local Nusselt variation figure for the last case shows that it is maximum at the ends of the source and minimum exactly at its center (verified in our work). For similar considerations, Aydin *et al.* [5], studied the problem for a Rayleigh number ranging from 10^{+3} to 10^{+6} and four lengths of the source (SL = 1/5 → 4/5 compared to side length). By means of numerical simulations and experimental measurements, Calcagni *et al*. [6] considered the same problem. Results are in consistence with those in [4, 5]. The experimental measurements confirm the observations recorded for the local Nusselt evolution for different Rayleigh number and SL. Sarris *et al*. [7], dealt with the bottom heating of a glass melting tank, assuming an imposed thermal flux on a centered source. Rayleigh number from 10^{+2} to 10^{+7} has been assumed for SL ranging from 0.1-0.5. Results for both dynamic and thermal fields in addition the exchange rate were presented, specifying the situations that best promote glass fusion. For a rectangular cavity with different values of the aspect ratio (L/H), in addition the possibility of inclination, the excellent rich work of Sharif *et al.* [8] is recommended. The results show the increase in mean Nusselt number with the increase of the aspect ratio and the tilting angle and its decrease with the increase of the source length. For more results in the same axis, the work of Saha *et al*. [9] can be viewed.

For a *non-Newtonian* power-law fluid, we cite the work of Raisi [10]. Several source lengths were assumed (from 0.2-0.8). Three values of the rheological index n (0.6, 1.0, and 1.8) were taken overall, except for the result $\overline{\mathrm{Nu}}(n)$ achieved with more n values. For the Rayleigh number (Ra_n), four values were considered (10^{+3}, 10^{+4}, 10^{+5} and 10^{+6}). Results show the increase in perturbations with increasing Ra_{n} as expected and their decrease with increasing n due to increasing fluid viscosity. As a consequence, an increasing average Nusselt with Ra_n and decreasing with n is obtained. Despite the interesting results presented. The large spacing between the values taken for each of the influencing parameters, left gaps for the best analysis of their effects. An extension of this work can be viewed in [11]. In an excellent and highly recommended work recently published by Yigit *et al.* [12], the cooling of a centered source under *imposed temperature* is studied. A source length from 0.2- 0.8, Ra_n from 10^{+3} to 10^{+6}, and n from 0.6-1.8 for Pr_n = 1000 were assumed. The effect of Pr_{n} was lastly studied, taking a range of its variation between 10 and 1000. Rich results with good quality that comply with ours were presented. This work with that published by Horimek

et al. [13] treating moreover the effect of cavity tilting for source length equal 1.0, help to well understand the effects of n, Ra_n, and Pr_n.

As already mentioned, the present work is a continuation of that recently published by Horimek *et al.* [1], where the confined fluid is now non-Newtonian described by the power-law model. The idea is to analyze the contribution of the viscosity change on the heat exchange rate by taking the same considerations taken in [1]. It is important to note that this rheological model includes three types of fluids (shear-thinning, Newtonian and shear-thickening), hence its importance, especially when the geometric aspect (*SL* and *D*) has a great effect. In addition, we will assume the case with the *imposed temperature* heating condition as principal and which will benefit of more results' presentation, unlike what we did previously. Consulting both of them will therefore, offer a maximum of understanding.

From the consulted literature, it can be said that the non-Newtonian effect for a decentered source under imposed temperature condition and that of Pr_n for both heating types were not treated. Likewise, Great limitations in the values assumed for the various intervening parameters in particular *SL* and *D*, especially for cavity' top under T_C condition. The aforementioned limitations will be extensively treated in addition other improvements compared to what was published.

Problem description

The problem dealt with is the cooling of a heat source of variable length and position, placed at the bottom of a square cavity by means of natural-convection. The cavity is filled with a power-law non-Newtonian fluid. Vertical walls and the upper one are under low temperature, while the remaining parts in the lower wall are insulated. Two types of uniform heating are assumed for the source: *imposed temperature* or *imposed flux density,* fig. 1. The flow is assumed to be laminar with constant physical properties except for density and viscosity. The problem is therefore, 2-D and Cartesian. Prandtl number is taken equal to 1000, except when its effect is studied at the end.

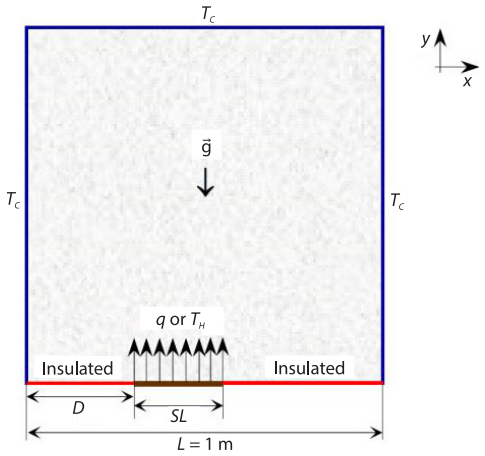

Figure 1. Geometry and details

With the previous details and by adopting Boussinesq' hypothesis, the equations of the problem are:

$$\frac{\partial u}{\partial x}+\frac{\partial v}{\partial y}=0 \tag{1}$$

$$u\frac{\partial u}{\partial x}+v\frac{\partial u}{\partial y}=-\frac{1}{\rho_{\mathrm{ref}}}\frac{\partial p}{\partial x}+\frac{1}{\rho_{\mathrm{ref}}}\left(\frac{\partial \tau_{xx}}{\partial x}+\frac{\partial \tau_{xy}}{\partial y}\right) \tag{2}$$

$$u\frac{\partial v}{\partial x}+v\frac{\partial v}{\partial y}=-\frac{1}{\rho_{\mathrm{ref}}}\frac{\partial p}{\partial y}+\frac{1}{\rho_{\mathrm{ref}}}\left(\frac{\partial \tau_{xy}}{\partial x}+\frac{\partial \tau_{yy}}{\partial y}\right)+\mathrm{g}\beta\left(T-T_{\mathrm{ref}}\right) \tag{3}$$

$$u\frac{\partial T}{\partial x}+v\frac{\partial T}{\partial y}=k\left(\frac{\partial^2 T}{\partial x^2}+\frac{\partial^2 T}{\partial y^2}\right) \tag{4}$$

where u and v are the velocity components in the x- and y-directions. p, β, g, k, and T – the pressure, thermal expansion coefficient, gravity acceleration, thermal conductivity, and temperature, respectively, and ref index indicates that the values are evaluated at the reference temperature, T_C.

For a non-Newtonian fluid, the viscosity is no longer constant inside the cavity. Different mathematical (rheological) models describing its variation have been published in the literature, see for instance [14]. In our study, the Ostwald-De-Waele model is considered. This model is given:

$$\tau = \mu_a \dot{\gamma} = K \dot{\gamma}^{n-1} \tag{5}$$

where μ_a is the apparent viscosity, K – the consistency, $\dot{\gamma}$ – the shear rate, and n the power-law index.

This expression encompasses three types of fluid. Shear-thinning fluid (or pseudoplastic) for $n < 1$; Shear-thickening fluid (or dilatant) for $n > 1$, and Newtonian fluid ($\mu_a = K \equiv \mu$) for $n = 1$.

The fluid rheological nature, directly affects the flow shape (its circulation), and thus, temperature field and heat transfer rate. Hence, the reformulation of the representative dimensionless numbers in this kind of problems is essential. Many concepts can be found in literature [15]. In this work, we have assumed the modified Rayleigh and Prandtl numbers:

$$\mathrm{Ra}_n\big|_{\mathrm{T}} = \frac{g\beta L^{2n+1}(T_H - T_C)}{\alpha^n \left(\frac{K}{\rho}\right)}, \quad \mathrm{Ra}_n\big|_{\mathrm{q}} = \frac{g\beta L^{2n+2} q}{k\,\alpha^n \left(\frac{K}{\rho}\right)}, \quad \mathrm{Pr}_n = \frac{K}{\rho}\alpha^{n-2} L^{2-2n} \tag{6}$$

The aforementioned expressions, eq. (7), are obtained from a scale analysis of the viscosity [16].

Cavity' side length L equals 1.0 m is taken as characteristic length for SL and D.

Boundary conditions

$$\begin{gathered}
(x = 0 \text{ or } L, y): u = v = 0\ ;\ T = T_C \\
(x, y = L): u = v = 0\ ;\ T = T_C \\
\left(x = [0\ ; D] \text{ and } [D + SL\ ;\ L], y = 0\right):\ u = v = 0;\ \frac{\partial T}{\partial y} = 0 \\
\left(x = [D\ ;\ D + SL], y = 0\right):\ u = v = 0\ ;\ \frac{\partial T}{\partial y} = q/k \ \text{ or } T = T_H
\end{gathered} \tag{7}$$

To quantify heat exchange rate intensity, Nusselt number should be calculated. We define the local one Nusselt number and the mean one Nusselt number. These two numbers are calculated using the expressions:

$$\mathrm{Nu}\big|_{\mathrm{T}} = \left.\frac{\partial \theta}{\partial y}\right|_{y=0}, \quad \mathrm{Nu}\big|_q = \frac{qL}{T_{\text{source}} - T_C}, \quad \overline{\mathrm{Nu}} = \frac{1}{SL}\int_D^{D+SL} \mathrm{Nu}\,\mathrm{d}x \quad \left[\theta = \frac{T - T_C}{T_H - T_C}\right] \tag{8}$$

Resolution procedure

The problem governing equations are solved numerically using a finite volume code following the SIMPLE algorithm [17]. A second-order central differencing scheme is used for

the diffusive terms, while a second-order up-wind scheme is used for the convective terms. Convergence residual values are chosen 10^{-6} for mass and momentum and 10^{-9} for energy. The choices are motivated by the flow perturbations caused by n decrease, Ra_n increase and source length and position. It should be noted that for the case with $SL = 0.1$ and $n = 0.6$ we took 10^{-5} instead of 10^{-6} with a finer mesh following some difficulties of convergence (long calculation time consumed).

Mesh study

In order to choose the optimal mesh ensuring excellent accuracy/minimum computation time, fig. 2, a study was carried out, assuming an equidistant mesh in both directions (x, y) progressively refined from 100 × 100 to 180 × 180. A comparison was then made with a carefully chosen non-uniform mesh, very refined on the source and close to the walls. The comparison is made by taking $n = 0.6$, $Ra_n = 10^{+6}$, $Pr_n = 1000$, $SL = 0.4$, and $D = 0.15$, reflecting a very strict case. By comparing the velocity and temperature fields in addition the average Nusselt number, the optimal mesh coincides perfectly with the very refined equidistant one (180×180) with more than 25% of reduction in computation time.

Finally, the optimal mesh characterized by: $\Delta y = 1/140$, for the source: $\Delta x_S = 1/200$ and for the insulated parts $\Delta x_{in} \approx 1/150$ is used for simulations.

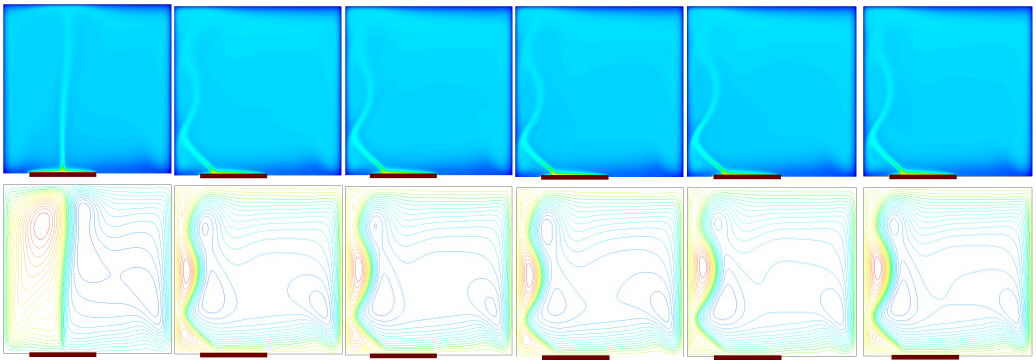

Figure 2. Mesh ($N_x \times N_y$) refinement effect and comparison with the optimal mesh; imposed temperature; $n = 0.6$; $Ra_n = 10^{+6}$, $Pr_n = 10^{+3}$, $SL = 0.4$, $D = 0.15$; top: temperature and bottom: stream function

Validations

Once the optimal mesh has been chosen, lots of validations were made with published works to rely on the results obtained here not yet published. Only one validation will be presented by limitation of space. This later, made with the work of Raisi [10], is devoted to the thermal field, θ_{max} and $\overline{Nu}$ for three values of n (0.6, 1.0, and 1.4) for the case of source under imposed flux density condition on the far left ($D = 0.0$), with $Ra_n = 10^{+5}$ and $Pr_n = 100$, fig. 3. Excellent agreements were obtained.

Results and discussion

In order to better exploit the obtained results and to well illustrate the effects of the numerous influencing parameters, this part of the work is divided into three parts. In the first,

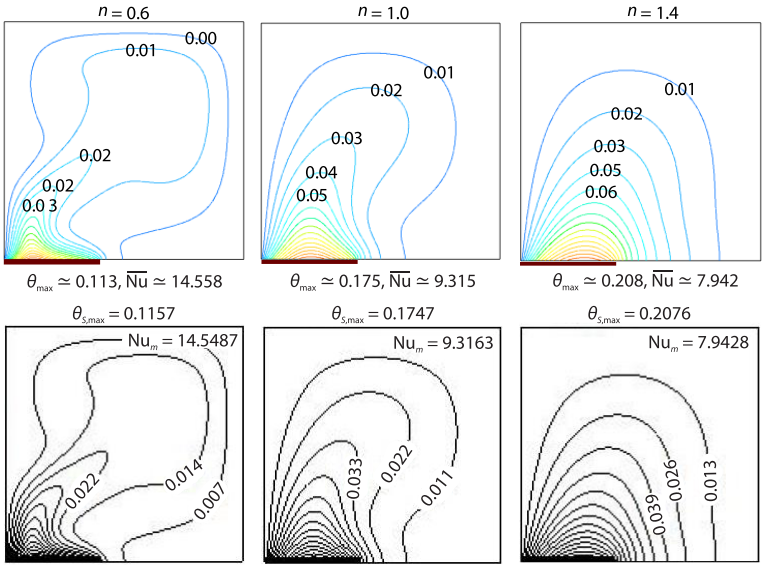

Figure 3. Validations for temperature field for *SL* = 0.4 and *D* = 0.0 for different *n* values; imposed flux density; $Ra_n = 10^{+5}$, $Pr_n = 10^{+2}$; top: our results and bottom: results of [12]

we present for the case of a centered source, the effects of SL and *n* for $Ra_n = 10^{+4}$ and 10^{+6} for imposed temperature case then imposed flux density case. The results are those for the dimensionless dynamic, ψ, and thermal, θ, fields, local Nusselt number and finally mean Nusselt number. In the second, the case of an off-centered source is presented by analyzing the effect of the distance *D* for different SL and *n*. For this case, we took $Ra_n = 10^{+5}$ for both heating types. For both parts, Prn is taken equal 1000. In the third part and for a centered source only, the effect of Pr_n is analyzed by considering a large range of its variation (from 5.0-10000).

Centered source: Effects of SL and rheological index, n

For this first part, six source lengths were assumed (SL = 0.1, 0.2, 0.4, 0.6, 0.8, and 1.0), which include very short, medium and long source. For the rheological index *n*, we took five values (0.6, 0.8, 1.0, 1.2 and 1.4) including shear-thinning, Newtonian, and shear-thickening fluid, respectively. The *n* = 1.4 is taken as the greatest value, since very weak changes occur for greater values that can be avoided entirely to conserve space, see [6, 9, 11, 12, 15] for verification). For Ra_n, we took two values for dynamic and thermal fields (10^{+4} and $10^{+}6$), while lots of values were taken when drawing $Nu(Ra)_n$. The two values were chosen by the fact that they represent weak and strong natural-convection intensities, respectively. Interested reader on the effect of Ra_n on dynamic and thermal fields can refer to [1, 15, 18]:

– Imposed temperature case

Figure 4 shows the effects of SL and *n* on the dimensionless dynamic (stream function) and thermal (isotherms) fields for $Ra_n = 10^{+4}$ and $Ra_n = 10^{+6}$. The Newtonian case (*n* = 1.0) placed in the middle can serve as a witness on the effect of the index *n*. From fig. 4(a), one can see from the temperature sub-figures a concentration of the hot fluid close to the source (red and orange zones) as expected, a gradual decrease is observed moving away from the source until the cold walls (dark blue for the lowest temperature T_C). In addition, the amount of heat entering from the source directly depends on its size (its length). This is the reason for recording larger

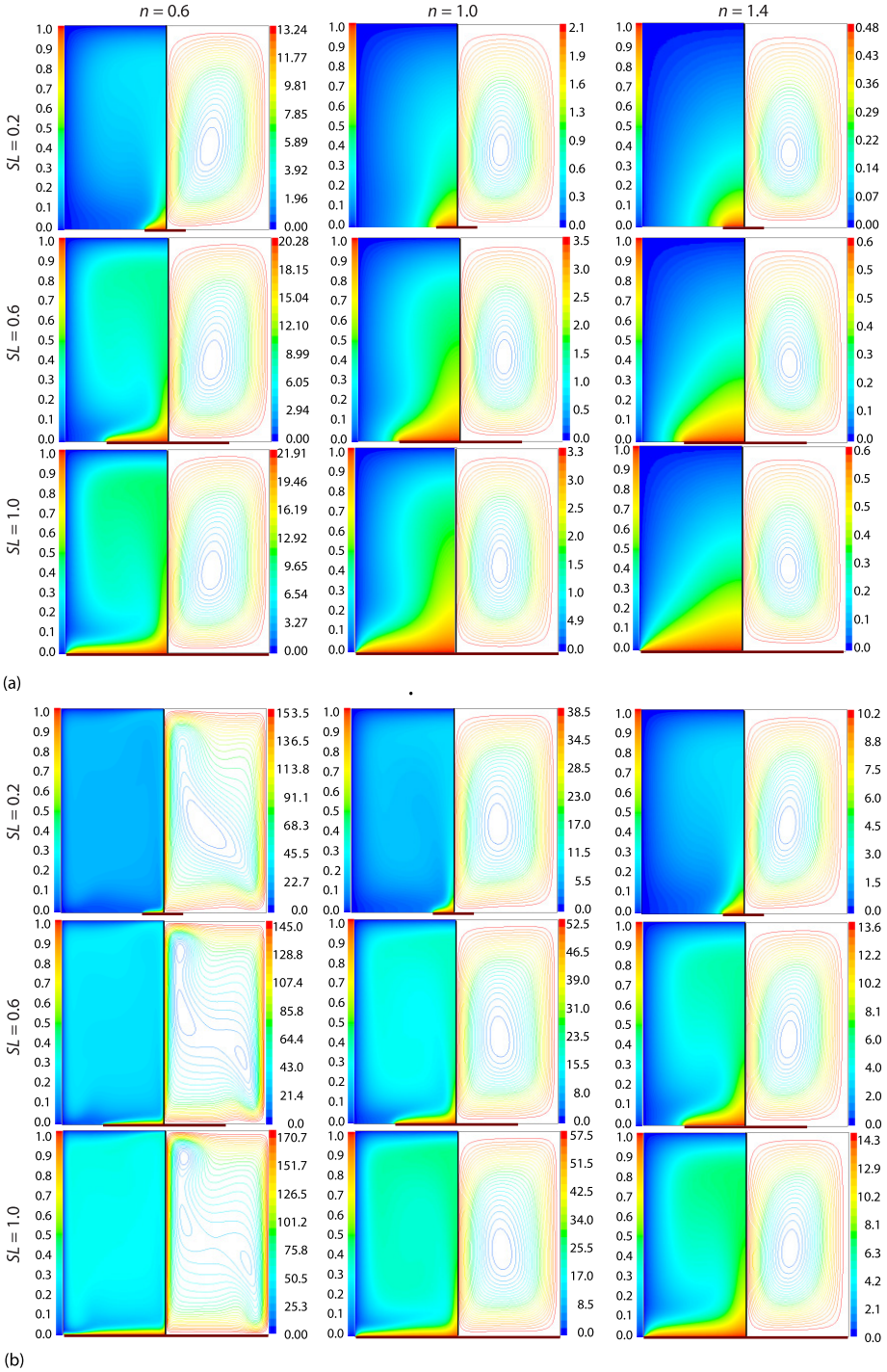

Figure 4. Isotherms (left half) and streamlines (right half) for different SL, n, and Ra_n; $Pr_n = 10^{+3}$; imposed temperature and centered source; (a) Ra = 10^{+4} and (b) Ra = 10^{+6}

hot zones when SL increases for the same n and even Ra_n [1, 12]. This can be observed on the intensities of the stream-function (see captions). An exception from SL close to 0.6 and greater reflected by the stability of stream-function intensity level is observed. It can be explained by the fact that the hot fluid' high speed level reached following the strong heating will generate larger perturbation in the cavity after its rising until the top wall and division on both sides of the symmetry plane. In other words, there is a reduction in maximums of fluid circulation due to the enlargement in disturbed areas (greater mixing). The rheological index n also has a clear influence on both fields. Compared to the Newtonian case, there is an increase in convection intensity when n decreases and the reverse when increases. The shrinking effect is more noticeable for large SL than for small ones. But, we must mention the effect of n even at small SL, where we can see the upward extension of the areas of ascending hot fluid more narrowed when n is small compared to when it is large, which can be considered as favoring of convection *vs*. conduction. This is the reason that we see hotter zones (light blue) at the top for $n = 0.6$ and SL = 0.1 with decreasing degree when n increases, where the hot fluid hardly reaches the upper parts. Good mixing will therefore, take place when n decreases and the opposite when it increases. The n effect becomes more intense when Ra_n increases as can be observed from fig. 4(b) for $Ra_n = 10^{+6}$. For this value, one notices advanced mixing levels for all n except for the cases of a dilatant fluid with small SL, see for $n = 1.4$ and $SL = 0.2$, where the braking by non-Newtonian nature of the fluid opposes the flow generated by natural-convection under small reduction in density due to the low incoming heat from the small source. Sub-figures analysis shows the displacement of the circulation zone upwards compared to the previous case with $Ra_n = 10^{+4}$ due to the intensification of the ascending upward flow. In addition, the circulation zone is oriented towards the symmetry plane when n becomes small (pseudoplastic case), because of the ascending hot fluids areas narrowing on and near it following the strong reduction in viscosity under the combined effects of n and $\dot{\gamma}$. As SL increases, the incoming heat amount increases and the area of density reduction widens. Perturbations (or mixing) are spread throughout the cavity, in particular at very small n, resulting in a multiplicity of circulation zones. The phenomena observed at small SL and $n \approx 0.6$ are observed for large SL and $n \geq 1.0$ at low Ra_n.

– Imposed heat flux density case

For this heating type, dynamic and thermal fields are presented in fig. 5. Overall, the results are similar to those for the *imposed temperature* case. In this case, source temperature changes along it, and its maximum is exactly at its center by symmetry. Hence, more decrease in density on and near the axis of symmetry that will reduce the diffusion of perturbations in the cavity. This can be seen by analyzing the two heating cases captions for the same considerations (SL, n, and Ra_n). By comparing the levels of circulation (amounts reached in the stream-functions), one notice that this type of heating gives lower intensities. In addition, the multiplicity of circulation zones, see fig. 5 for $SL = 0.6$ and 1.0 for $n = 0.6$) is no longer recorded. This is explained by the narrowing of the central zone (on the axis of symmetry) under the unequal distribution of temperature on the source. On the other hand, in the *imposed temperature* case, the source evenly heats the adjacent fluid layers, despite the influence of flow. As known to any specialist, the transition turbulent regime goes through a so-called transitional phase which begins with anarchic perturbations. By comparing for the aforementioned case (the one of comparison), one can predict that the transition will occur in the *imposed temperature* case before this heating case.

The Nusselt number evolution along the source for both heating types is presented in fig. 6. Three cases with different SL (0.2, 0.6, and 1.0) for $Ra_n = 10^{+6}$ and five values of n (0.6, 0.8, 1.0, 1.2, and 1.4) were considered. As expected, the increase in flow perturbation

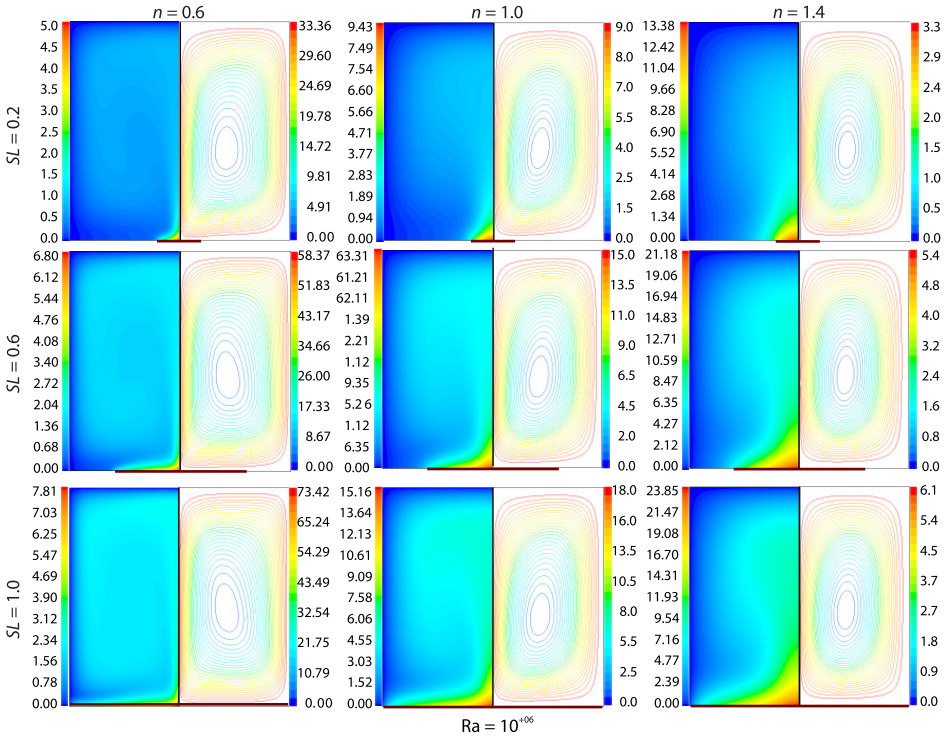

Figure 5. Isotherms (a) ($\times 10^{+2}$) and streamlines (b) for different SL, n, and Ra_n, $Pr_n = 10^{+3}$; imposed flux density and centered source

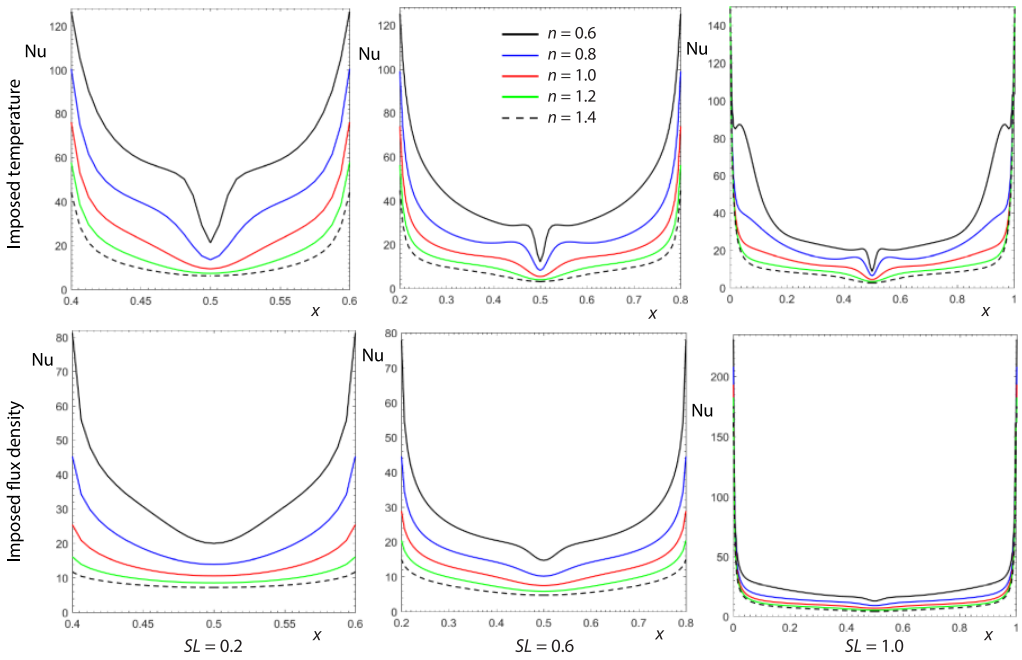

Figure 6. The Nusselt number evolution along the source for different n and SL, $Pr_n = 10^{+3}$, $Ra_n = 10^{+6}$; centered source

generates an increase in heat exchange rate, noting that imposed temperature heating type offers a greater Nusselt number compared to imposed flux density one, following the greater perturbation as detailed a little previously. The n decrease shows improvement of Nusselt number for any consideration, due to viscosity decrease that intensity flow circulation after friction reduction. Curves analysis shows that the maximum value of Nusselt number is at the source' ends while the minimum value is exactly at its center. This is explained by the fact that Nusselt number increases with the decrease in fluid temperature near the source, which allows the introduction of more heat flux from it, and since the maximum temperature is exactly at the source' center, the minimum of Nusselt number will be there and vice versa at the ends of the source.

In fig. 7, $\overline{Nu}$ evolution as a function of Ra_n for both heating types is presented. Six SL values and five n values were considered. Twenty-five Ra_n values were taken for each case (10^{+3}, $1.25 \cdot 10^{+3}$, $2.5 \cdot 10^{+3}$, $5 \cdot 10^{+3}$, $6.25 \cdot 10^{+3}$, $7.5 \cdot 10^{+3}$, $8.75 \cdot 10^{+3}$, 10^{+4},…, 10^{+6}) to ensure good precision and good smoothing of the lines. As expected, $\overline{Nu}$ increases with increasing Ra_n following the rise of convection intensity. In addition, one can see that for all cases, there is a point of passage from a purely horizontal curve (zero slope) to an inclined curve. The first part reflects a negligible intensity of natural-convection. By analyzing the curves for $n = 0.6$ for imposed temperature case, one observes an exception, where the sensitivity to Ra_n change starts too early, which is not surprising given the strong decrease in viscosity which reduces the opposition the weak intensity of natural-convection. For imposed flux density case, this result is recorded only for large SL due to the centralization of the higher temperature on the symmetry axis. The minimum value of $\overline{Nu}$ (horizontal part) changes with SL and likewise for higher values (inclined part), where a strong $\overline{Nu}$ is recorded for $SL = 0.1$, followed by a gradual decrease as SL increases and finally a rise for $SL = 1.0$. This result has been well detailed in [1, 12] for a Newtonian fluid. Same observations are recorded when n changes with increase in $\overline{Nu}$ as n decreases. For the reason already detailed, $\overline{Nu}$ is stronger in the first heating type compared to the second for all considerations.

Non-centered source: effect of source position

In this part, the source is no longer centered. It is distant from the left vertical wall of D, counted up to the left end of the source, review fig. 1. It is obvious that D changes with SL. Noting that the large number of parameters makes impossible to assume all their variations. For this, we took a single value for Ra_n equal to 10^{+5} which is high enough to ensure intense convection and small enough to work quietly in laminar. The resemblance in dynamic and thermal fields between the two heating types, allowed us to present only those for *imposed temperature* case. Three values of SL (0.1, 0.4, and 0.8) were considered for the same previous n values, fig. 8. For each SL, three positions for the source were taken, on the far left ($D = 0.0$), in the middle (almost) and in the center, to clearly illustrate the effect of D. It is obvious that symmetry is lost in dynamic and thermal fields when the source is decentered, particularly when D is smaller. For $SL = 0.1$ (likewise for small SL), one observes a *main* circulation zone and *another* at the top left with current running in the opposite direction. This zone is all the larger as n decreases where its size is close to the *main* circulation zone for $n = 0.6$. For $n = 1.0$, a *third* zone of small size is recorded above the source, also rotating in the opposite direction. If one take the case with $n = 1.0$ as reference, one can explain the circulation shape. The density decreases near the source, an upward movement of the hot fluid is generated, to its left, the ascending fluid finds the static wall that slows it down, while on its right, it is totally of fluid easy to be sheared. Therefore, the main generated flow moves to the right because friction is lower. As the cavity is completely filled, circulation is created in the upper left by motion continuity. The small cir-

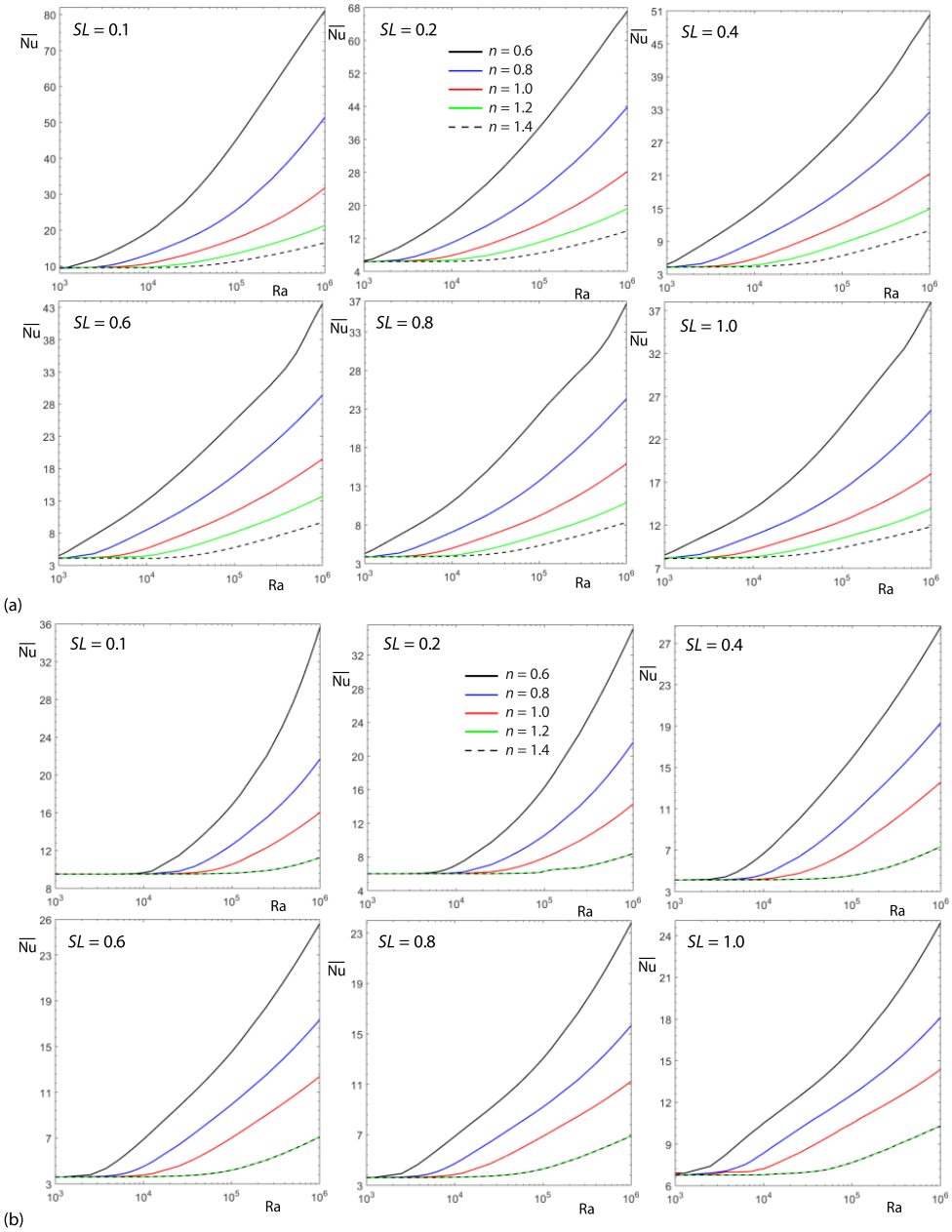

Figure 7. The $\overline{Nu}$ evolution *vs.* Ra_n number for different *n* and SL, $Pr_n = 10^{+3}$; centered source; (a) imposed temperature and (b) imposed flux density

culating area on the source is not observed when Ra_n is small as amply detailed in [1], fig. 10 and explanation, where the opposite circulating area runs from bottom to top. So, the third zone is a step between a spread zone in addition the main zone, and two large opposite zones when Ra_n becomes important, that will strongly disturb the fluid in almost all the cavity. Due to the fact that *n* reduction leads to movement intensification, the third circulating zone is no longer

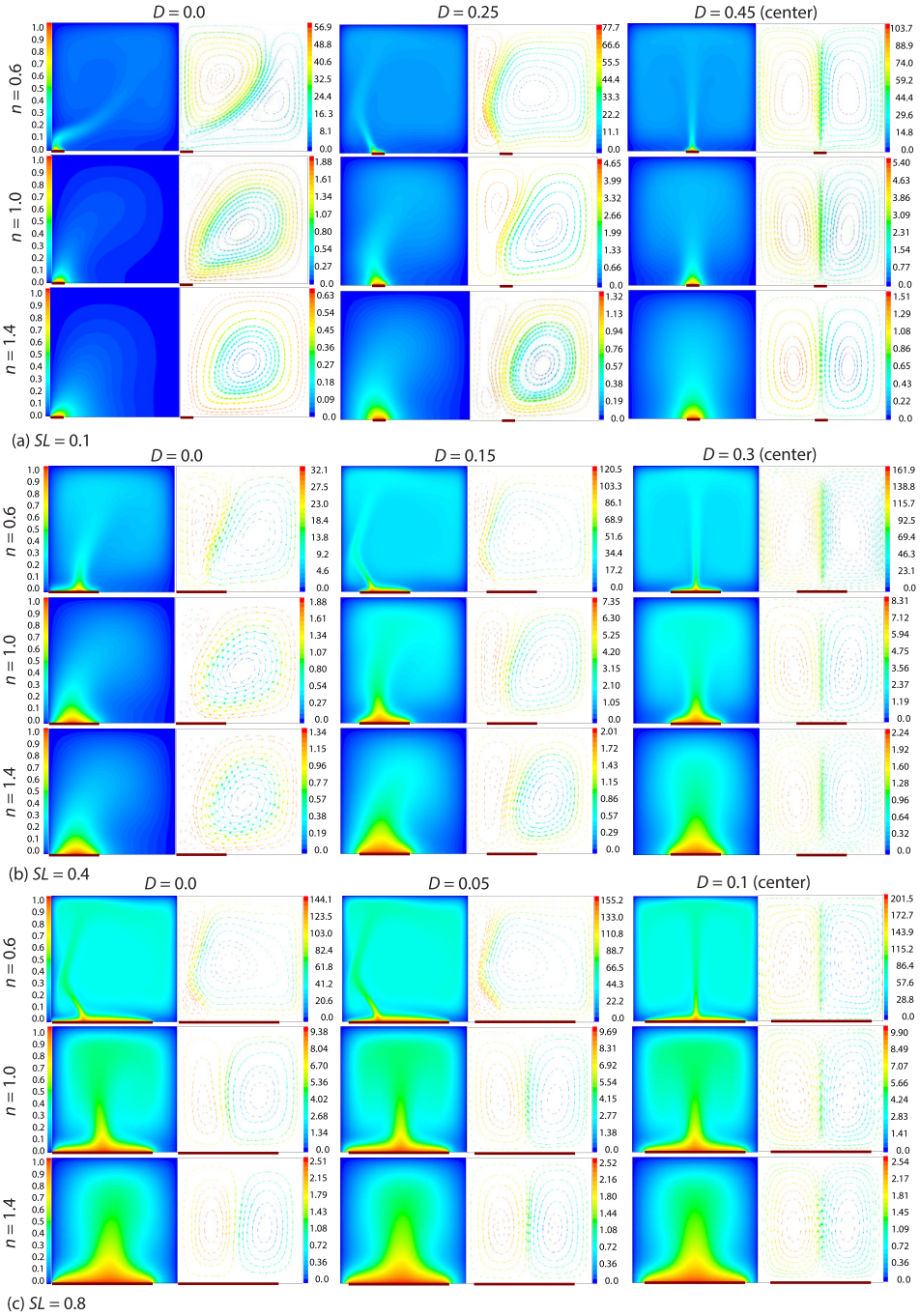

Figure 8. The *D* effect on dynamic and thermal fields for different *n* and SL, $Ra_n = 10^{+5}$, $Pr_n = 10^{+3}$; imposed temperature; (a) *SL* = 0.1, (b) *SL* = 0.4, and (c) *SL* = 0.8

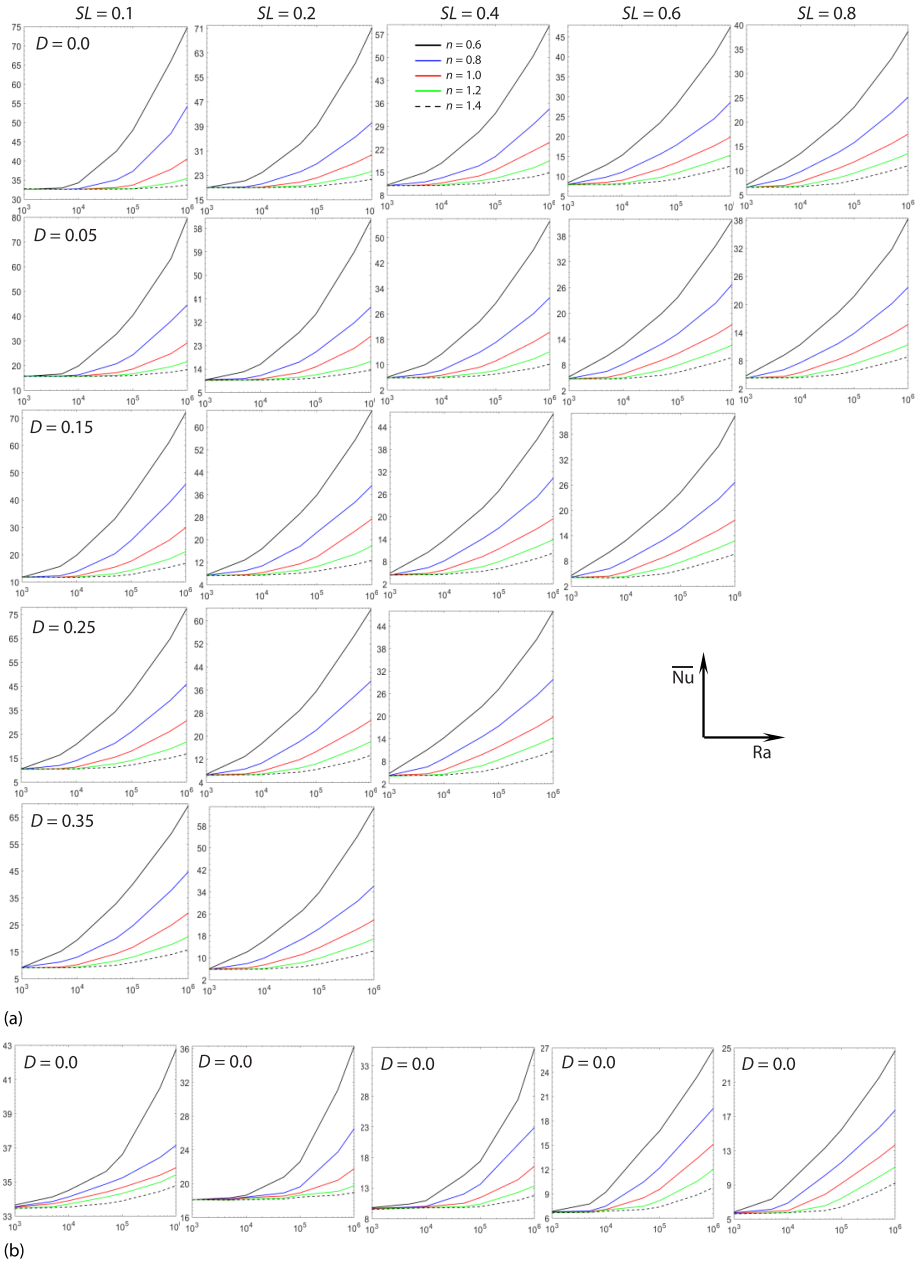

Figure 9. The $\overline{\mathrm{Nu}}$ evolution *vs.* Ra_n number for different D, n, and SL , $\mathrm{Pr}_n = 10^{+3}$; (a) imposed temperature and (b) imposed flux density

observed for $n = 0.6$, in addition the widening of the second zone when n decreases. When increasing D, rising hot fluid left side is no longer a wall. Thus, flow slowing down decreases with D until reaching symmetry. Temperature field presents the same observation by problem coupling nature. The same observations are recorded when SL increases with the exception of

non-presence of the third circulating zone, which is simply explained by the large area of decrease in fluid density for big SL, and hence clearer intensification of circulation.

The Nusselt number variation was not presented intentionally, because of the loss of symmetry which makes its presentation useless. For this reason, only D effect on $\overline{\mathrm{Nu}}$ evolution is presented in fig. 9(a) for imposed temperature case. It is noted that for this case, thirteen values of Ra_n were taken instead of twenty-five as done for a centered source case. The reason for this limitation is the very large number of simulations to be carried out. From the sub-figures, the greatest values of $\overline{\mathrm{Nu}}$ are recorded for $D = 0.0$ for all the simulated SL, notably for $n \geq 1.0$. This is well observed for weak Ra_n, while for large Ra_n the large $\overline{\mathrm{Nu}}$ values obtained for $n = 0.6$ require careful analysis. A review of [1] fig. 11, is highly recommended specifying that $\mathrm{Pr} = 0.71$ in the reference. The high values obtained (for $D = 0.0$) are mainly due to the T_C condition on the left wall, which results in improved heat extraction and therefore, more flux entering from the source. As specified, this result is noted the most for weak Ra_n with $n \geq 1.0$, two situations that favorite conductive heat exchange which shows an important role for the left wall condition. As Ra_n increases and/or n decreases, D effect becomes less important on $\overline{\mathrm{Nu}}$ because of high convection intensities in these cases (Ra_n high and n small) in addition good thermal field mixing.

As recorded for the centered-source case, when SL increases $\overline{\mathrm{Nu}}$ decreases gradually. This remains valid when D increases. But one cannotice by analyzing the sub-figures of fig. 9(a) that the decay is more pronounced for $n < 1.0$ than for $n \geq 1.0$. This is explained by intensity reduction of convection when n increases, what will keep the phenomena recorded in the Newtonian case ($n = 1.0$) valid for the case of dilatant fluid ($n > 1.0$) with smaller amounts. For a pseudoplastic fluid ($n < 1.0$), the high sensitivity of the flow to viscosity reduction, leads first to record significant heat exchange levels, in addition a clearer reduction when SL increases. It must always be remembered that the viscosity decay under n effect will increase $\dot{\gamma}$ and therefore, a strong reduction in viscosity. In addition, when moving vertically then horizontally on fig. 11(a), it can be noted that SL effect is more important than that of D (compare the reached amounts). Same observations are recorded for the case of imposed flux density heating, fig. 9(b), with lower $\overline{\mathrm{Nu}}$ amounts. It is noted that only results for $D = 0.0$ and all SL have been presented for this case, to allow comparison with imposed temperature case and imposed flux density case for a centered source.

Prandtl number effects

For this last part, Pr_n effect will be presented. Given the large number of parameters involved in the problem, we took only $\mathrm{Ra}_n = 10^{+5}$, and $n = 0.7$, 1.0 and 1.3 for a centered source. The Pr_n considered values are 5, 10, 50, 100, 500, 1000, 5000, and 10000, which encompasses a very wide range of variation. It should be noted that for $\mathrm{Ra}_n = 10^{+6}$, we did not succeed in stabilizing the code after several various interventions for $\mathrm{Pr}_n < 5.0$ for the *imposed temperature* case only. In what follows, temperature field for $SL = 0.4$ will be presented for both heating types, Then $\overline{\mathrm{Nu}}(\mathrm{Pr}_n)$ evolution. Obviously at this stage of the work, no need to extend results for lots of SL, interested reader can review [1]. The Pr_n number depicts the ratio between motion diffusion, υ, and heat diffusion, α. Its growth is therefore, ensured when the first increases and/or the second decreases. The υ increase will widen the zone disturbed by the flow generated by convection under viscous friction effect. Likewise, α reduction reduces the inertia to heat diffusion within the filled cavity.

From there, one can well understand the results of the increase of Pr_n on the thermal field presented in fig. 10. Even more, we can understand that Pr_n effect will be clearer when Ra_n

is large, see [1, 12], by opposed effects of υ (check from Pr_n and Ra_n expressions), especially when n is small. Consequently, temperature field clearly changed as Pr_n increases for $n = 0.7$, a little for $Pr_n = 1.0$ and almost insensitive to its change for $n = 1.3$ for both heating types. One can see from the sub-figures when $n = 0.7$, the reduction in size of the high temperature zones close to the source and the enlargement of the medium temperature zones sizes when Pr_n becomes important compared to the case for $Pr_n = 5.0$. It can easily be concluded that heat exchange will improve when Pr_n increases as a result of cooling on and near the source, which will ensure a greater temperature gradient between the source and the adjacent fluid layers. By comparing the two heating types, one can see that Pr_n effect is more pronounced in *imposed temperature* case than the other due to greater generated perturbations as explained previously, hence a clearer Pr_n effect when changed. It is obvious that this observation will remain valid for all SL and D.

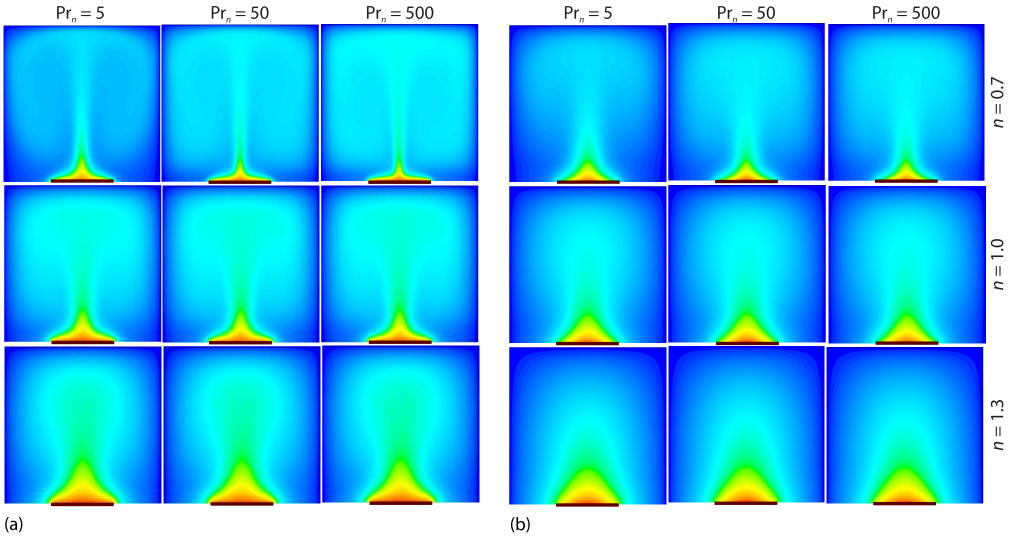

Figure 10. The Pr_n effect on the thermal field for different n, $SL = 0.4$, $Ra_n = 10^{+5}$; centered source; (a) imposed temperature and (b) imposed flux density

In fig. 11, $\overline{Nu}$ evolution with the increase of Pr_n is presented. Three SL for each type of heating were chosen (0.1, 0.2, and 0.4 for *imposed temperature*; 0.6, 0.8, and 1.0 for *imposed flux density*). The curves of evolution confirm the observation on the thermal field, fig. 10, and our explanation. One can see the non-sensitivity to Pr_n change for $n = 1.3$, small sensitivity for $Pr_n < 50$ (or even < 10) for $n = 1.0$ only, while the change is very clear for $n = 0.7$ even for high values de Pr_n. By comparing the two heating types ($SL = 0.4$ for the first and $SL = 0.6$ for the second are close each other), one can observe that the improvement in $\overline{Nu}$ when Pr_n increases is faster in the first heating type as explained previously when we talked about its effect on the thermal field. In addition, this improvement is more extensive (spreads to large Pr_n values) for this type compared to the second.

Conclusions

The results obtained from this study led to conclude are as follows.

- For a centered source:
  - The Ra_n increase, SL increase and n decrease intensify dynamic and thermal field perturbations with clearer amounts for the imposed temperature case then imposed flux density one.

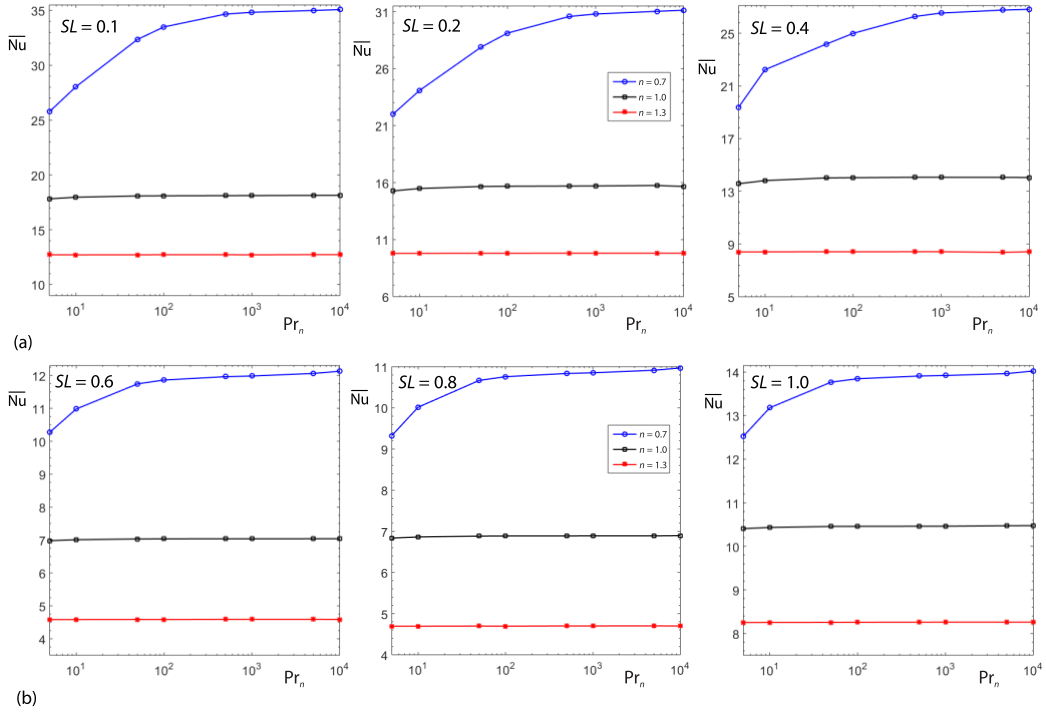

Figure 11. The Pr_n effect on $\overline{Nu}$ for different n and SL, $Ra_n = 10^{+5}$; centered source; (a) imposed temperature and (b) imposed flux density

  - The Ra_n increase improve local and mean heat transfer rates, while SL increase is accompanied by a decrease in the mean exchange rate with an exception for $SL = 1.0$ due to boundary conditions.
  - For all situations, n effect is present, especially when it is small (<1.0), expressed by strong intensities. The opposite is recorded when it is big (>1.0).

- **For a non-centered source**
  - The symmetry observed for the previous source position is absent in this case. Its absence is all the more pronounced when D, SL and n are small, especially at strong Ra_n.
  - Bringing the source closer to the side wall increases the mean exchange rate. A maximum is recorded when $D = 0.0$ for all considerations;

- **The Pr_n effect**
  - The Pr_n increase widens heat diffusion area, hence a reduction in temperature close to the source. Wider thermal perturbations are recorded. The n decrease clearly amplifies Pr_n effect notably for the first type of heating (imposed temperature). Consequently, heat exchange improvement is recorded with the increase of Pr_n. This is clear and clean for $n < 1.0$, on the other hand very little felt for $n \geq 1.0$.
  - The effect of n when it is small spreads out for the first type of heating to very large Pr_n, while it is stopped early in the second type, $O(100)$.

Nomenclature

c_p – specific heat, [Jkg^{-1}K^{-1}]
D – distance between the source left extremity and the vertical left side, [m]
g – gravity acceleration, [ms^{-2}]
k – thermal conductivity, [Js^{-1}m^{-1}K^{-1}]
L – cavity side length, [m]
n – rheological index
Nu – local Nusselt number $((\partial\theta/\partial y|_{y=0})_T$; $=(qL/T_{\text{source}} - T_C))|_q)$
$\overline{\text{Nu}}$ – mean Nusselt number $(1/SL]_D^{D+SL}\text{Nud}x)$
p – pressure, [Kgm^{-1}s^{-2}]
Pr – Prandtl number $(= \mu c_p/k)$
q – heat flux density, [Js^{-1}m^{-2}]
Ra – Rayleigh number $(= (g\beta L^{2n+1}(T_H - T_C))$ / $(\alpha^n(K/\rho))|_T$; $=(g\beta L^{2n+2}q)/(k\alpha^n(K/\rho))|_q)$
SL – source length, [m]
T – temperature, [K]
u – x-velocity component, [ms^{-1}]
v – y-velocity component, [ms^{-1}]
x – x-co-ordinate, [m]
y – y-co-ordinate, [m]

Greek symbols

α – thermal diffusivity, [m^{2}s^{-1}]
β – thermal expansion coefficient, [K^{-1}]
θ – dimensionless temperature
μ – viscosity, [Kgm^{-1}s^{-1}]
ρ – fluid density, [Kgm^{-3}]

Subscript

C – cold
H – hot
q – imposed flux density
n – modified (for non-dimensional numbers for a non-Newtonian fluid)
ref – reference
T – imposed temperature

References

[1] Horimek, A., *et al.*, Natural-Convection Cooling of a Heat Source Placed at the Bottom of a Square Cavity. Effect of source Length, Position, Thermal Condition and Prandtl Number, *International Journal of Heat and Technology, 38* (2020), 3, pp. 722-737
[2] Rahal, S., *et al*., Numerical Study of Natural-Convection in a Cavity Filled with Air and Heated Locally from Below, *International Journal of Applied Mathematics Computer Science*, *5* (2017), 1, pp. 20-24
[3] Banerjee, S., *et al*., Natural-Convection in a Bi-Heater Configuration of Passive Electronic Cooling, *International Journal of Thermal Science*, *47* (2008), 11, pp. 1516-1527
[4] Seddiki, M. N., *et al.*, Effect of Buoyancy Force on the Flow Field in a Square Cavity with Heated from Below, *International Journal of Discrete Mathematics*, *2* (2017), 2, pp. 43-47
[5] Aydin, O., *et al*., Natural-Convection in Enclosures with Localized Heating from Below and Symmetrical Cooling from Sides, *International Journal of Numerical Methods in Heat and Fluid-Flow*, *10* (2000), 5, pp. 519-529
[6] Calcagni, B., *et al*., Natural Convective Heat Transfer in Square Enclosures Heated from Below, *Applied Thermal Engineering*, *25* (2005), 16, pp. 2522-2531
[7] Sarris, I., *et al.*, Natural-Convection in Rectangular Tanks Heated Locally from Below, *International Journal of Heat Mass Transfer*, *47* (2004), 14-16, pp. 3549-3563
[8] Sharif, M. A. R, *et al*., Natural-Convection in Cavities with Constant Flux Heating at The Bottom Wall and Isothermal Cooling from the Side Walls, *International Journal of Thermal Science*, *44* (2005), 9, pp. 865-878
[9] Saha, G., *et al*., Natural-Convection in Enclosure with Discrete Isothermal Heating from Below, *Journal of Naval Architecture and Marine Engineering*, *4* (2007), 1, pp. 1-13
[10] Raisi, A., Natural-Convection of Non-Newtonian Fluids in a Square Cavity with a Localized Heat Source, *Journal of Mechanical Engineering Science*, *62* (2016), 10, pp. 553-564
[11] Pishkar, I., *et al*., Numerical Study of Unsteady Natural-Convection Heat Transfer of Newtonian and Non-Newtonian Fluids in a Square Enclosure under Oscillating Heat Flux, *Journal of Thermal Analysis and Calorimetry*, *138* (2019), Apr., pp. 1697-1710
[12] Yigit, S., *et al*., Free Convection of Power-Law Fluids in Enclosures with Partially Heating from Bottom and Symmetrical Cooling from Sides, *International Journal of Heat Mass Transfer*, *145* (2019), 118782
[13] Horimek, A., *et al*., Laminar Natural-Convection of Power-Law Fluid in a Differentially Heated Inclined Square Cavity, *Annales de Chimie -Science des Materiaux*, *41* (2017), 3-4, pp. 261-28
[14] Bird, R. B., *et al.*, *Dynamics of Polymeric Liquids*, V.1, Fluid Mechanics, 2nd ed., Wiley, New-York, USA, 1987

[15] Khezzar, L., *et al.*, Natural-Convection of Power Law Fluids in Inclined Cavities, *International Journal of Thermal Science*, *53* (2012), Mar., pp. 8-17
[16] Turan, O., *et al*., Laminar Natural-Convection of Power-Law Fluids in a Square Enclosure Submitted From Below to a Uniform Heat Flux Density, *Journal of Non-Newtonian Fluid Mechanics*, *199* (2013), Sept., pp. 80-95
[17] Patankar, S. V., *Numerical Heat Transfer and Fluid-Flow, Hemispher*, Washington, USA, 1982

Paper submitted: May 31, 2022
Paper revised: September 17, 2022
Paper accepted: November 3, 2022